INDIAN JOURNAL OF SCIENCE AND TECHNOLOGY

ORIGINAL ARTICLE

Influence of AgCl Doping on Physical, Optical and Electrical Properties of Lithium-Borate Glasses

Ashok Mastanappa[1], M N Chandrashekara[2], G B Devidas[1]*, T Sankarappa[3], Shrikant Biradar[1,4], Shidaling Matteppanavar[5], R Ramanna[5]

1 Department of Physics, Kuvempu University, Shankaraghatta, Shivamogga – 577 451, Karnataka, India
2 Department of Physics, Sahyadri Science College, Shivamogga - 577 203, Karnataka, India
3 Department of Physics, Gulbarga University, Kalaburagi-585106, Karnataka, India
4 Department of Physics, Shri Shripadbodh Swamiji Government First Grade College, Mudalagi, 591 312, Karnataka, India
5 Department of Physics, KLE Society's Basavaprabhu Kore Arts, Science and Commerce College, Chikodi - 591 201, Karnataka, India

OPEN ACCESS

Received: 14/09/2025
Accepted: 15/10/2025
Published: 16/11/2025

Citation: Mastanappa A, Chandrashekara MN, Devidas GB, Sankarappa T, Biradar S, Matteppanavar S, Ramanna R (2025) Influence of AgCl Doping on Physical, Optical and Electrical Properties of Lithium-Borate Glasses. Indian Journal of Science and Technology 18(41): 3279-3291. https://doi.org/10.17485/IJST/v18i41.1582

* **Corresponding author**.

devidasgb02@gmail.com

Funding: None

Competing Interests: None

Published By Indian Society for Education and Environment (iSee)

ISSN
Print: 0974-6846
Electronic: 0974-5645

Abstract

Objectives: In order to investigate physical, optical, and conductivity properties, glasses were prepared with the composition (59-x) B_2O_3-25Li_2O-15CaF_2-1V_2O_5-xAgCl (x = 0-1.6 mol%, step 0.4). **Methods**: The glasses were prepared via melt quenching procedure at 1323 K. The glassy (non-crystalline) nature of the prepared samples was affirmed using X-ray diffraction (XRD) studies. The physical characteristics, including molar volume (V_m) and density (ρ_g), were computed at room temperature. By building Tauc's plots using UV-Vis. absorption, it was possible to determine the direct and indirect optical energy band gaps. **Findings**: The density rose from 2.426 to 2.493 g/cm^3, while the molar volume declined slightly from 25.585 - 25.366 cm^3/mol with AgCl addition. XRD confirmed the amorphous nature, optical analysis revealed a reduction in direct and indirect band gaps, with a slight increase at 1.6 mol% AgCl doping. This narrowing is attributed to structural modifications by AgCl nanoparticles, enhancing electron localization and donor centers in the glass network. Dielectric and AC conductivity measurements showed an enhancement in σ_{ac} from 2.328$\times$10^{-6} to 4.375$\times$10^{-6} Ω^{-1}m^{-1}. **Novelty**: The investigation of optical properties and electrical conductivity in novel alkali-borate glasses doped with AgCl nanoparticles demonstrates improved conductivity and optical performance, highlighting their potential for optoelectronic applications.

Keywords: Borate glasses; Ag-NPs; Band-gaps; Dielectric properties; AC conductivity

1 Introduction

Glass formation primarily depends on the presence of a suitable glass former, such as SiO_2, P_2O_5, TeO_2, and B_2O_3. Among these, B_2O_3 stands out due to its exceptional glass-forming ability. In this study, borate glass was chosen owing to its excellent

chemical durability, optical transparency, and thermal stability making it a suitable candidate for a variety of advanced applications such as laser, display, and thermal sensors etc. Incorporation of modifiers, typically alkali or alkaline earth metal oxides, into borate glasses is found to improve the durability and reduce the moisture-absorbing characteristics of the resulting amorphous framework. Therefore, lithium oxide (Li_2O) is employed as a network modifier, which facilitates the transformation of tri-coordinated BO_3 units into tetra-coordinated BO_4 units, leading to the formation of additional bridging oxygens (BOs), thereby influencing the overall electrical conductivity of the glass and making the material well-suited for lithium-ion battery applications [1], [2].

Metal nanoparticles embedded glasses have drawn considerable attention because of their practical benefits. Incorporation of silver nanoparticles (Ag-NPs) into glass matrices can enhance emission efficiency and transparency useful in photonic devices applications of solar cells and optical switches. Furthermore, rather than displaying multifunctional behavior, each noble metal catalyst demonstrates activity that is unique to a given reaction. Therefore, in order to achieve trifunctional activity for use in water electrolyzers driven by rechargeable metal-air batteries, various catalysts with different catalytic characteristics must be hybridized [3], [4]. Additionally, Ag-NPs uniquely promote electrical conductivity when incorporated into borate glasses, since silver ions are not strongly bound to lattice sites or anion cages; they possess considerable freedom of movement [**5-6**]. AgCl is quite differing from Ag, when AgCl is incorporated into lithium-borate glass and melted; it partially dissociates according to $AgCl \rightarrow Ag^+ + Cl^-$. The released Ag^+ occupies modifier sites within the glass network, coordinating with non-bridging oxygens (NBOs) to form Ag-O linkages, while Cl^- ions may interact with boron to create Cl-B bonds. This process increases the NBO concentration and modifies the local structural environment. In contrast, when metallic Ag is directly introduced, it does not dissolve readily into the glass matrix during melting. Due to its weak interaction with the glass network and absence of bonding with oxygen, metallic Ag predominantly exist as phase-separated clusters rather than forming chemical bonds within the glass structure. Amorphous oxide materials incorporating transition metal cations (TMCs), like vanadium pentoxide (V_2O_5), attract significant attention owing to their semiconducting behavior. The addition of CaF_2 reduces the viscosity and liquidus temperature of the glass thereby enhancing optical clarity, further tailoring it for advanced optical applications.

AC conductivity analysis provides crucial insights into the conduction mechanisms, primarily arising from the motion of thermally activated mobile charge carriers [5]. This behavior is strongly influenced by changes in composition and temperature, which alter the density and mobility of these charge carriers, thereby modulating the material's overall conductivity response [6].

Various research studies have provided valuable insights into the electrical and optical features of Ag-NPs incorporated borate glasses. Notably, **Nur Adyani Zaini et al**. [7] conducted a comprehensive analysis focusing on the structural and optical characteristics of borate-based glasses infused with vanadium and Ag-NPs. Their findings revealed that increasing dopant concentration led to a decline in optical band gap and increase in Urbach energy and refractive index. **Keshavamurthy et al**. [8] explored the enhancement of structural attributes and photoluminescence intensity in the visible and infrared transitions of borate glasses following the incorporation of Ag-NPs. **Abhiram Jagannathan et al.** [9] have extensively explored the structural properties, refractive index enhancement, and nonlinear optical behavior of lithium fluoroborate glasses doped with Ag nanoparticles. To date, several studies have investigated the incorporation of silver nanoparticles into various glass matrices, revealing diverse structural and optical properties. However, there remains a significant gap in the literature regarding the quantification of AC electrical conductivity and analyzing the underlying conductivity mechanisms specifically in lithium-borate glasses doped with silver chloride (AgCl) nanoparticles containing calcium fluoride (CaF_2) and vanadium pentoxide (V_2O_5) within the *same* host glass matrix. The present study addresses this gap by examining the opto-electrical response of a novel glass material with the chemical composition (59-x) B_2O_3-25Li_2O-15CaF_2-1V_2O_5-xAgCl (x = 0-1.6 mol%, step 0.4). To this end, the UV-Vis spectroscopy is utilized to evaluate optical characteristics, while dielectrics properties and ac conductivity to understand electrical performance.

2 Methodology

2.1 Synthesis of the glasses

Glasses with the desired chemical composition (59-x) B_2O_3 - 25Li_2O- 15CaF_2- 1V_2O_5- xAgCl (x = 0-1.6 mol%, step 0.4) were produced following the melt-quenching technique. Analytically pure starting substances with 99.9% purity (supplied by M/S LOBA Chemie), including H_3BO_3, Li_2CO_3, CaF_2, V_2O_5, and AgCl, were measured in specified ratios, blended, and finely powdered with the help of an agate mortar and pestle to confirm a consistent blend. This uniform blend was moved into a ceramic crucible and subjected to heating at 1323 K inside an electrically powered muffle furnace. To ensure the formation of an amorphous structure, the resultant melt was transferred onto a brass plate surface and rapidly cooled to room temperature [10], [11]. The glass pieces were subsequently heat-treated at 573 K to alleviate internal residual stresses and designated as BAg-0, BAg-1, BAg-2, BAg-3, and BAg-4 and visual representations are provided in Figure 1.

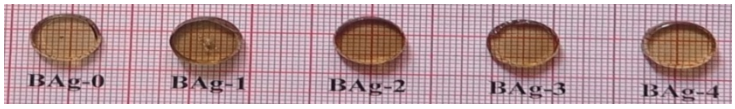

Fig 1. Photograph of prepared samples

2.2 Characterizations used

2.2.1. X-ray diffraction (XRD) and Calculation of physical properties

The finely ground glass materials were investigated using X-ray diffraction (XRD) conducted over a 2Θ range of 10°–90° with the help of a Rigaku Smart Lab diffractometer with Cu-Kα radiation (λ=1.54 Å). For physical property evaluation, the density (ρ_g) of the glass samples was examined employing Archimedes' principle utilized toluene as immersion liquid, using a high-precision microbalance (SCALE-TECH) with an accuracy of ±0.001g. The following formulas were used to calculate the ρ_g and V_m of the glasses:

$$\rho_g = \left(\frac{Wa}{W_a - W_L}\right) x\, \rho_L \tag{1}$$

$$V_m = \frac{M_W}{\rho_g} \tag{2}$$

Here, ρ_L represents the density of toluene (0.866 g/cm^3); and M_W denotes the molecular weight of the glass composition as calculated based on its molar constituents[12].

Ion concentration (N_{Ag}), polaron radius (r_p), inter-ionic separation (r_i), field strength (F) and oxygen packing density (OPD) were determined using following equations[13]:

$$N_{Ag} = \frac{X\%\, x\, \rho_g x\, N_A}{M_W} \tag{3}$$

$$r_p = \frac{1}{2}\left(\frac{\pi}{6N}\right)^{1/3} \tag{4}$$

$$r_i = \left(\frac{1}{N}\right)^{1/3} \tag{5}$$

$$F = \frac{Z}{(r_p)^2} \tag{6}$$

$$OPD = n\, x \left(\frac{\rho_g}{M_W}\right) x1000 \tag{7}$$

Here, X% stands for the additive concentration, Z for AgCl's atomic number, N_A for Avogadro's constant, and n for the number of oxygen atoms present in a single molecular formula unit of the glass.

2.2.2. Investigation of UV-Visible absorption

A Shimadzu UV-Vis spectrophotometer (model: UV-2600) was used to record the glasses' optical properties within a wavelength range of 200–1000 nm. Using the obtained absorbance A(λ) and sample thickness (t) as variables, **Eqn. (8)** was used to derive the optical absorption coefficient α(v). Tauc's approach was employed to assess the optical energy band gaps (E_{gap}), as stated in **Eqn. (9)**[14],[15].

$$\alpha(\nu) = \frac{2.303A(\lambda)}{t} \tag{8}$$

$$\alpha h\nu = B\left(h\nu - E_{gap}\right)^{m} \tag{9}$$

Where m = 1/2 and m =2 correspond to direct and indirect transitions, respectively.

The Urbach energy was calculated using **Eqn. (10)**.

$$\alpha(\nu) = \beta exp\left(\frac{h\nu}{E_U}\right) \tag{10}$$

Here, β denotes a proportionality factor (constant), hν signifies photon energy, and E_U corresponds to the Urbach tail energy.

The indirect optical energy band gap (E_{indir}) was used to determine the refractive index (μ) in accordance with Dimitrov-Sakka relation **(Eqn. 11)**[16]. Other key optical features including the dielectric constant (ε), reflection loss (R_L), optical transmittance (T), molar refraction (R_m), electronic molar polarizability (α_m), and metallization factor (M) were calculated using the subsequent following relations (**Eqn**. **12-17**).

$$\frac{(\mu^2-1)}{(\mu^2+2)} = 1 - \sqrt{\frac{E_{indir}}{20}} \tag{11}$$

$$\varepsilon = \mu^2 \tag{12}$$

$$R_L = \frac{(\mu^2-1)}{(\mu^2+2)} \tag{13}$$

$$T = \frac{2\mu}{\mu^2+1} \tag{14}$$

$$R_m = \frac{(\mu^2-1)}{(\mu^2+2)}\, x\, V_m \tag{15}$$

$$\alpha_m = \left(\frac{3}{4\pi N_A}\right) x\, R_m = \frac{R_m}{2.52} \tag{16}$$

$$M = 1 - \frac{R_m}{V_m} \tag{17}$$

2.2.3. Conductivity measurements

Glasses of definite dimensions were selected, and silver paste was applied on their top and bottom surfaces. Temperature readings were taken using a chromel-alumel thermocouple. To evaluate the dielectric characteristics, capacitance (C) and loss tangent (tanδ) were recorded utilizing a highly accurate impedance meter (Wayne Kerr 6520B) across a signal frequency span of 100 Hz to 3 MHz and a thermal interval of 373 K to 573 K. By using the following formulas, the dielectric constant (ε'), dielectric loss (ε''), and ac conductivity (σ_{ac}) were computed[17]:

$$\varepsilon' = \frac{Ct}{\varepsilon_0 A} \tag{18}$$

$$\varepsilon'' = \varepsilon' tan\, \delta \tag{19}$$

$$\sigma_{ac} = \omega \varepsilon_0 \varepsilon'' \tag{20}$$

Where ε_0 represents the permittivity of free space, tanδ indicates the phase difference between current and voltage with respect to the applied electric field, ω = 2πf (where f is the frequency), t denotes the thickness, and A refers to the glasses' area of cross-section.

3 Result and discussions

3.1 XRD analysis

The prepared samples' XRD patterns are shown in Figure 2, exhibiting a broad hump between 20° and 30°. The absence of sharp peaks or long-range order in these regions indicates a lack of crystalline structure confirming the glassy nature of the synthesized samples.

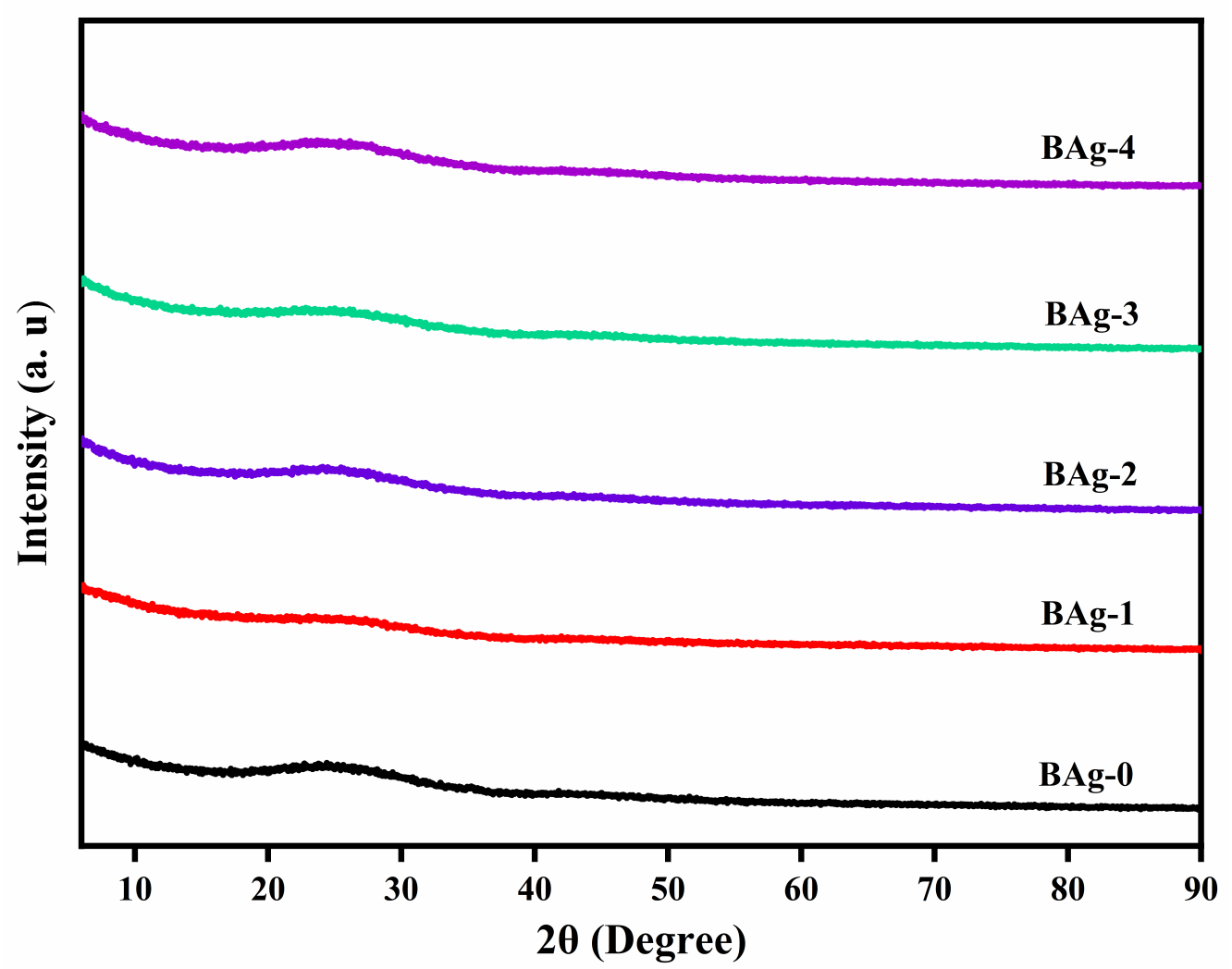

Fig 2. XRD profile of the prepared samples

3.2 Physical properties analysis

The physical parameters of the developed glasses are tabulated in Table 1. With AgCl doping, the density of the glasses rose from 2.426 to 2.493 g/cm^3, and the molar volume decreased from 25.585 to 25.366 cm^3/mol. The observed enhancement in density has been attributed to the transformation from triangular BO_3 units to tetrahedral BO_4 units, producing stronger bonds, and a more compact structure. Additionally, the replacement of lighter B_2O_3 (69.62 g/mol) by heavier AgCl (143.32 g/mol) also contributes to increase in density [13]. In the present glasses, the added Ag-NPs may occupy interstitial positions within the glass network, resulting in a reduction in glasses' molar volume leading to an augmentation in density and hence glasses' rigidity. The OPD was calculated, and the values are presented in Table 1. The increased OPD is consistent with the decline in molar

volume and the rise in density, indicating that the oxygen atoms are more compactly arranged within the glass network. This increased compactness stabilizes the glass structure**.**

Table 1. Physical parameters of BAg glasses

Glass sample codes	Density (x g/cm^3)$\pm$ 005	Molar volume (xcm^3/ mol) $\pm$ 004	Ion concentration (x10^{23} ion/cm^3)	Polaron radius (x10^{-9}cm)	Inter- nuclear distance (x10^{-9}cm)	Field strength (x10^{17}cm^{-2})	Oxygen packing density (OPD) (mol/cm^3)
BAg-0	2.426	25.585	-	-	-	-	80.905
BAg-1	2.451	25.443	0.094	0.193	0.480	1.704	81.356
BAg-2	2.466	25.409	0.189	0.153	0.381	2.706	81.465
BAg-3	2.478	25.407	0.284	0.134	0.333	3.545	81.472
BAg-4	2.493	25.366	0.379	0.122	0.302	4.298	81.603

The additional parameters values, such as N_{Ag}, r_i, r_p, and F_s, are presented in Table 1, further validate that the glass network is indeed close-packed. The addition of Ag-NPs has increased N_{Ag} in the glass network, and their good dispersion within the glass matrix has resulted in a concurrent reduction in r_i and r_p. The crowding of Ag-NPs may have led to an increase in bond strength as a result of the stronger field strength around the Ag^{2+} ions[18].

3.3 Optical studies

The UV absorption spectra obtained is shown in Figure 3. The glasses without silver appeared light yellow and transparent, but with the addition of silver nanoparticles, they developed a slightly darker yellowish colour. The absorption decreases gradually as the wavelength increases, except for a notable and sharp increase at shorter wavelengths. The absence of sharp band edges indicates that the material is amorphous, as confirmed by XRD studies. The glasses' optical energy band gaps were evaluated utilizing Tauc's formula (**Eqn. 9**). Tauc's graphs of $(\alpha h\nu)^2$ and $(\alpha h\nu)^{1/2}$ versus $h\nu$ were extended to intercept the horizontal axis in order to compute both direct and indirect transitions[18]. The direct and indirect energy band gaps (E_g) values are obtained and presented in Table 2.

Table 2. Optical properties of the prepared glass samples

Optical properties	BAg-0	BAg-1	BAg-2	BAg-3	BAg-4
Direct band gap energy (eV) $\pm$ 001	3.129	3.063	3.051	3.013	3.060
Indirect band gap energy(eV) $\pm$ 001	3.006	2.986	2.977	2.958	3.005
Urbach energy(eV)	0.292	0.219	0.274	0.283	0.211
Refractive index (μ)	2.395	2.400	2.403	2.408	2.396
Dielectric constant (ε)	5.738	5.764	5.776	5.801	5.740
Reflection loss (R_L)	0.612	0.613	0.614	0.615	0.612
Optical transmission (T)	0.711	0.710	0.709	0.708	0.710
Molar refractivity (R_m) (cm^{-3})	15.666	15.612	15.606	15.636	15.847
Electronic polarizability (α_m)	6.216	6.195	6.193	6.205	6.288
Metallization criterion(M)	0.388	0.386	0.385	0.384	0.387

For the produced glasses' optical energy band gaps are shown graphically in Figures 4(a) and 4(b), which represent direct and indirect transitions, respectively. With increasing AgCl content from 0 mol% to 1.2 mol%, a progressive drop in the optical band gaps is observed. The decreased in direct band gap from 3.129 to 3.013 eV, while indirect band gap shows a slight decline from 3.006 to 2.958 eV. A similar trend has been observed for the same host matrix[19]. The narrowing in band gap is ascribed to structural modifications caused by AgCl nanoparticles addition, which promotes enhanced electron localization and an increase in donor centres within the glass network. The band gap values appear to be of similar magnitude, which may, in turn, be insignificant for manufacturing unique cut-off wavelength emitters and solid-state photodetectors operating in the UV–blue frequency range[18],[20],[21]. However, for the sample containing 1.6 mol% AgCl, a marginal anomalous increase in both direct and indirect band gaps is recorded, rising to 3.060 eV and 3.005 eV, respectively. This reversal suggests a reduced degree of electron localization and a diminished number of donor centres. These effects are probably caused by structural reorganisation in the glass matrix, specifically a reduction in the concentration of NBOs (non-bridging oxygens) and possibly AgCl phase

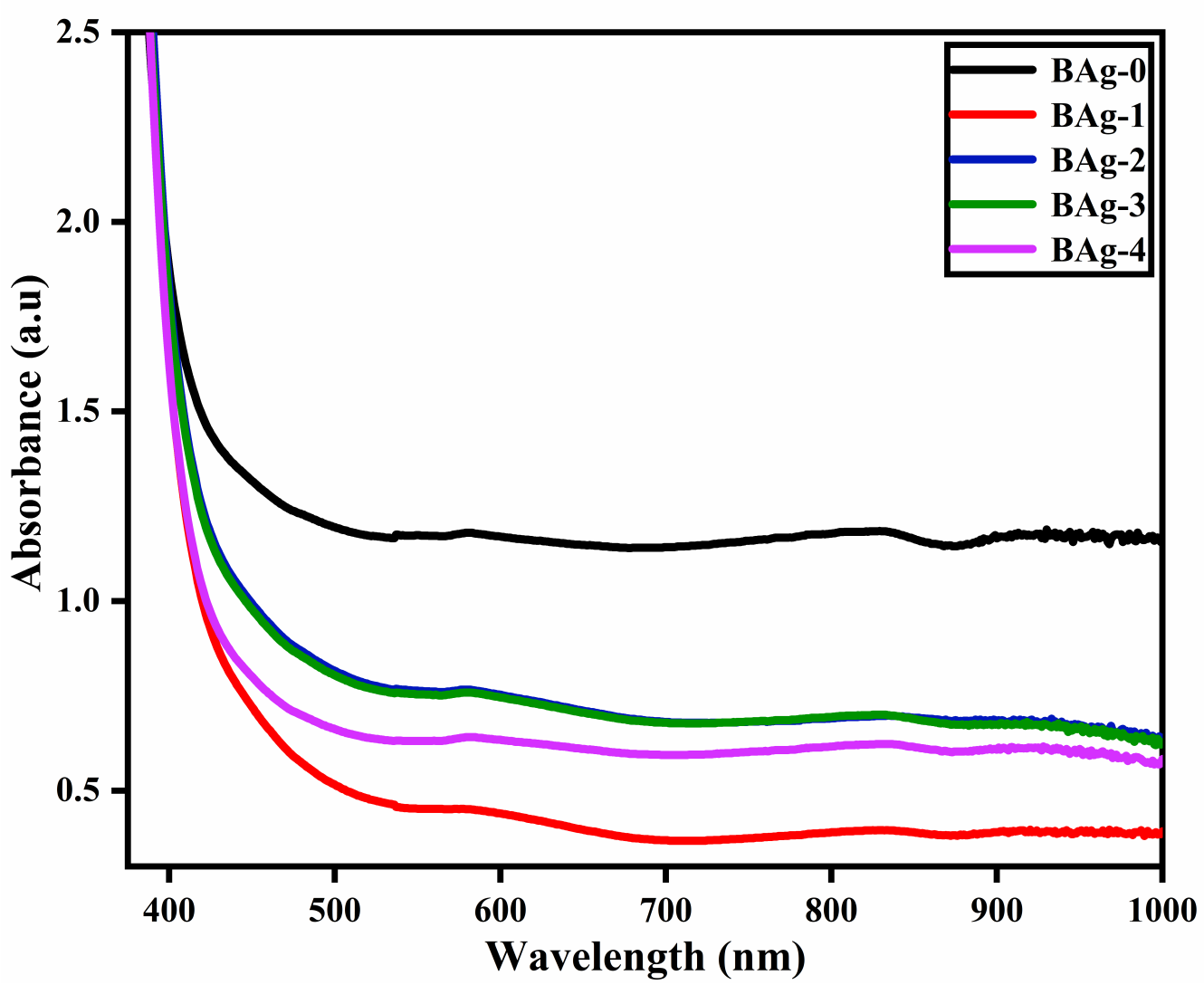

Fig 3. UV- Visible absorption spectra of the glasses

segregation at higher doping level. The Urbach energy (E_U) which quantifies the width of localized states and reflects the degree of structural disorder[18] was also evaluated. E_U values were determined by plotting ln(α) versus hν, where E_U is represented by the linear region's inverse slope as depicted in Figure 5. The variation in E_U values, listed in Table 2, correlates with the presence of structural imperfections induced by AgCl doping. The observed increase in E_U with rising AgCl concentration confirms greater disorder and disruption inside the glass network structure, and indicating the reduction in strength of the glass network[22],[23].

The synthesized glasses' refractive index (μ) was determined followed by the Dimitrov-Sakka relation (**Eqn. 11**), and the corresponding values are tabulated in Table 2. The results indicate a steady increase in μ from 2.395 to 2.408 as the AgCl mol% rises from 0 mol% to 1.2 mol% (BAg-0 to BAg-3). This enhancement in refractive index is attributed to the increased structural compactness of the glass matrix[19] and the higher polarizability introduced by AgCl doping. However, at 1.6 mol% AgCl loading (BAg-4), the refractive index slightly decreases to 2.396, which may be ascribed to a reduction in non-bridging oxygens (NBOs)[15]. The consistent high refractive index values (μ > 1.85) across all compositions suggest that these glasses possess promising potential for optoelectronic applications[12]. Furthermore, optical parameters such as (R_L), (T), (ε), (R_m), and (α_m) also increased for BAg-0 to BAg-3 glasses and slightly decreased for 1.6 mol% AgCl doped glass because they are directly depended on μ value**.** A key determinant of whether a material behaves in a metallic (conductive) or non-metallic (insulating) manner is the metallization parameter (M). This standard states that a compound is considered as non-metallic, if

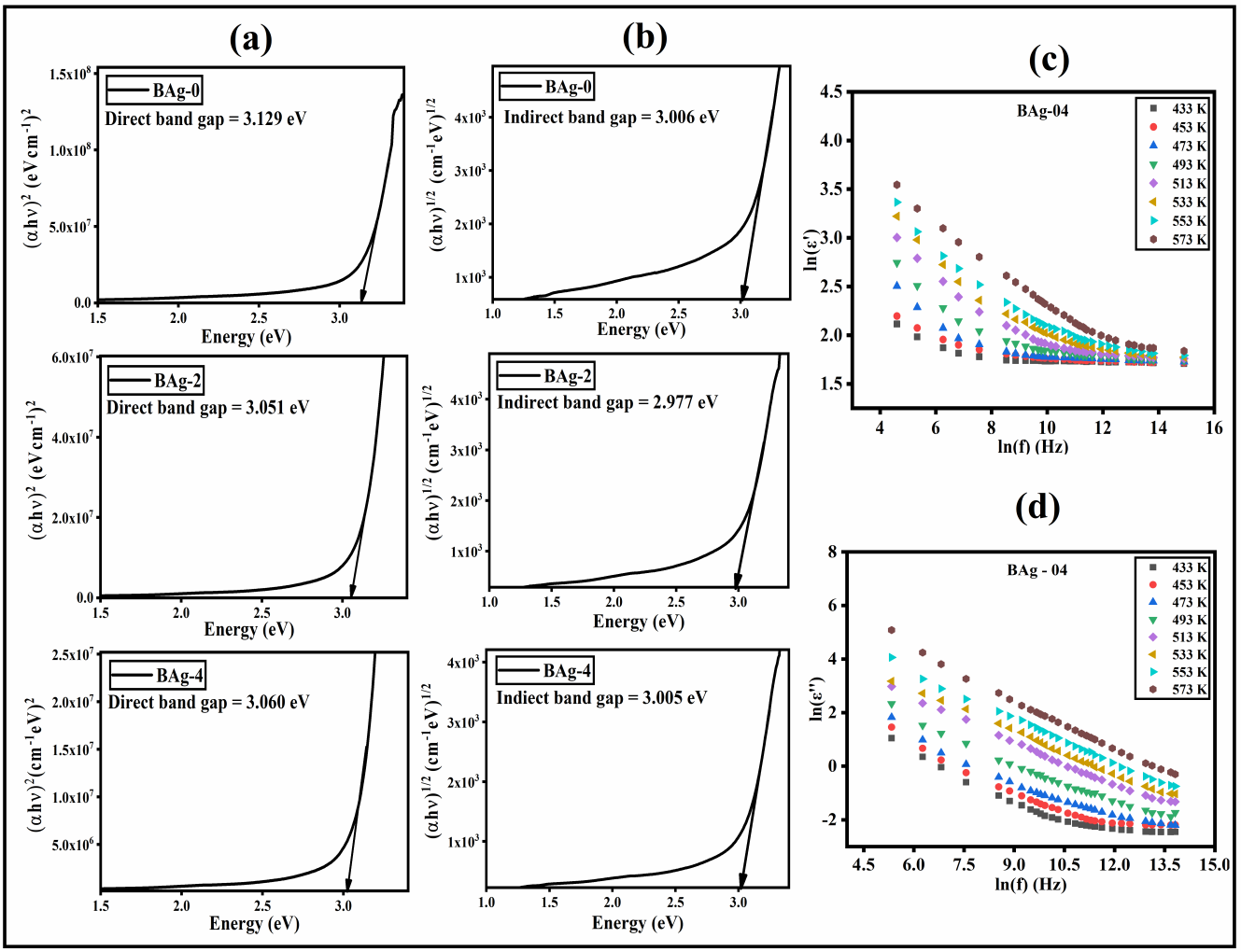

Fig 4. (a) and (b): Tauc's plots for finding the direct indirect band gap energies of the glasses (c): Plot of ln(ε') versus ln(f) for BAg-4 glass at different temperatures and (d): Plot ln(ε") versus ln(f) for BAg-4 glass at different temperatures

(R_m/V_m) < 1, and metallic if (R_m/V_m) > 1. The determined M values, which are shown in Table 2, show that (R_m/V_m) is less than 1, indicating that the glass samples under study are non-metallic[12].

3.4 Dielectric Properties

The dielectric properties are important; the dielectric constant (ε') reflects the material's ability to store electrical energy, whereas the dielectric loss (ε'') signifies the energy dissipated from the electric field inside the materials. ε' and ε'' of the present glasses exhibited noticeable variations with frequency, temperature, and dopant concentration. Figures 4(c) and 4(d) illustrate the variations of ε' and ε'', plotted against ln(f) at various temperatures for the BAg-4 glass. It is observed that both ε' and ε'' diminish as frequency and temperature increases. This kind of variation in ε' and ε'' has been observed for the other borate glasses[24]. This decline in ε' with frequency can be attributed to a decrease in orientation polarization at higher frequencies; the dipoles are unable to rotate quickly enough to follow the alternating electric field. As a result, the ε' decreases and stabilizes to a constant value at very high frequencies, due to only space charge polarization[17]. At low and moderate frequencies, the elevated dielectric loss values are linked to ionic hopping, conduction losses arising from ion transport, and ionic polarization. Conversely, at elevated frequencies, dielectric loss is primarily controlled by ionic oscillations, leading to a further decrease in ε''.

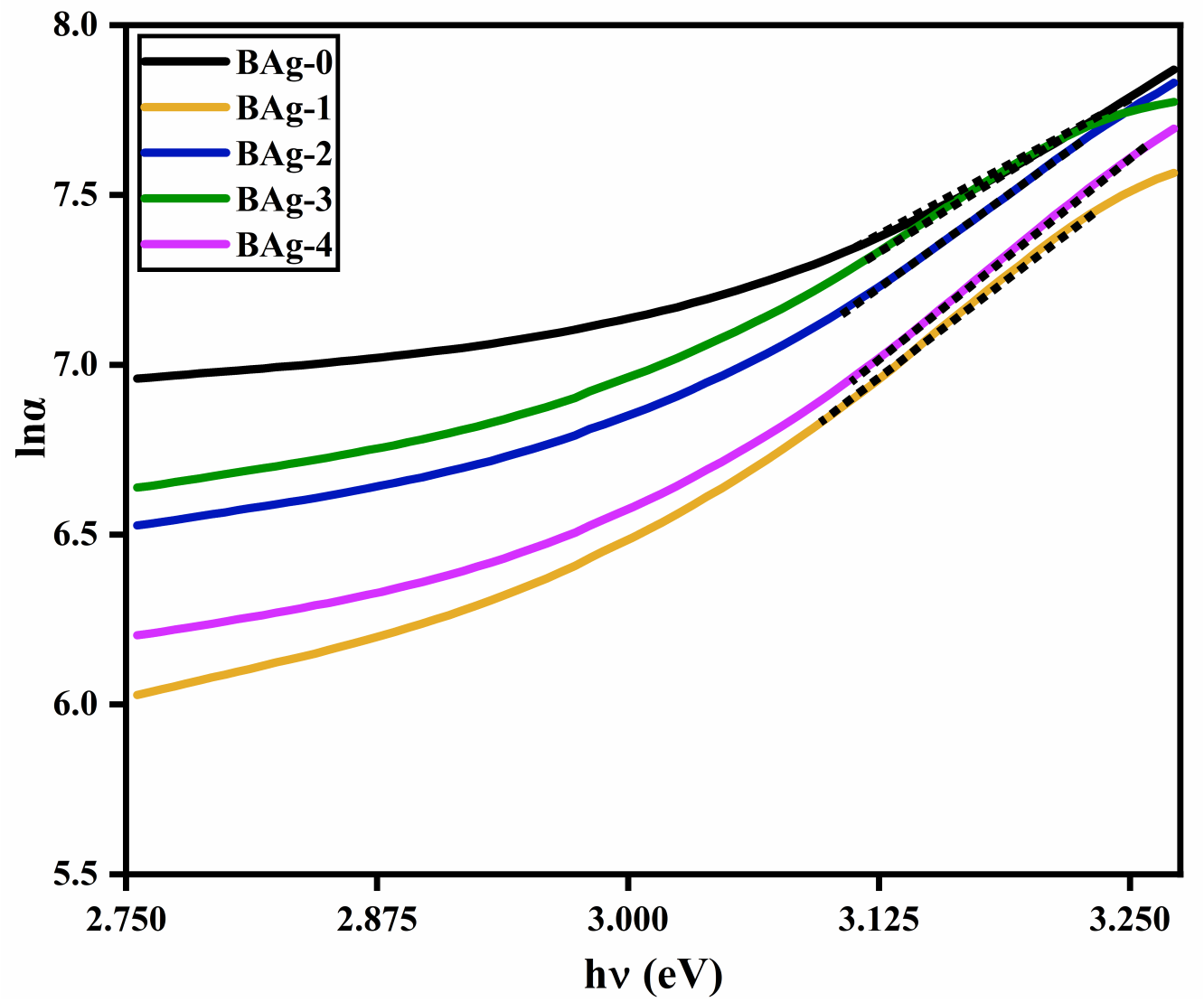

Fig 5. Plots of ln(α) versus (hν)

3.5 AC Conductivity

Understanding the electrical conduction of semiconductor materials under an applied AC electric field reveals important information about the mechanisms of charge transport and the arrangement of states within the forbidden gap. The total conductivity (σ_T), values for all the glasses were determined using the measured dielectric parameters, as per **Eqn. (20)**, σ_T can be considered as a sum of σ_{dc} and σ_{ac}. For the current glasses σ_T ranges from 2.215x10^{-5} to 1.065x10^{-4} (Ωm)$^{-1}$ between undoped and highest mol% of AgCl doped glasses at 500 kHz frequency. Figure 6 presents total conductivity (σ_T) of the BAg-4 glass sample. It is evident that the σ_T enhanced with both frequency and temperature. The measured values of σ_T across all the samples are in good agreement with those reported for alkali borate glasses [17]. At higher frequencies, the frequency dispersion is less noticeable than at lower frequencies. Additionally, it has been shown that when temperature rises, the high-frequency dispersion zone of AC conductivity significantly reduces. This behavior suggests a mechanism that is thermally activated and associated to an increase in charge carriers. As seen in Figure 6, the charge carriers drift across greater distances at lower frequencies due to the applied electric field [25].

The dc component is frequency-independent and dominates at lower frequencies, typically appearing as a flat region known as the dc plateau. This plateau, which signifies the dominance of dc conductivity, is discernible at higher temperatures. In

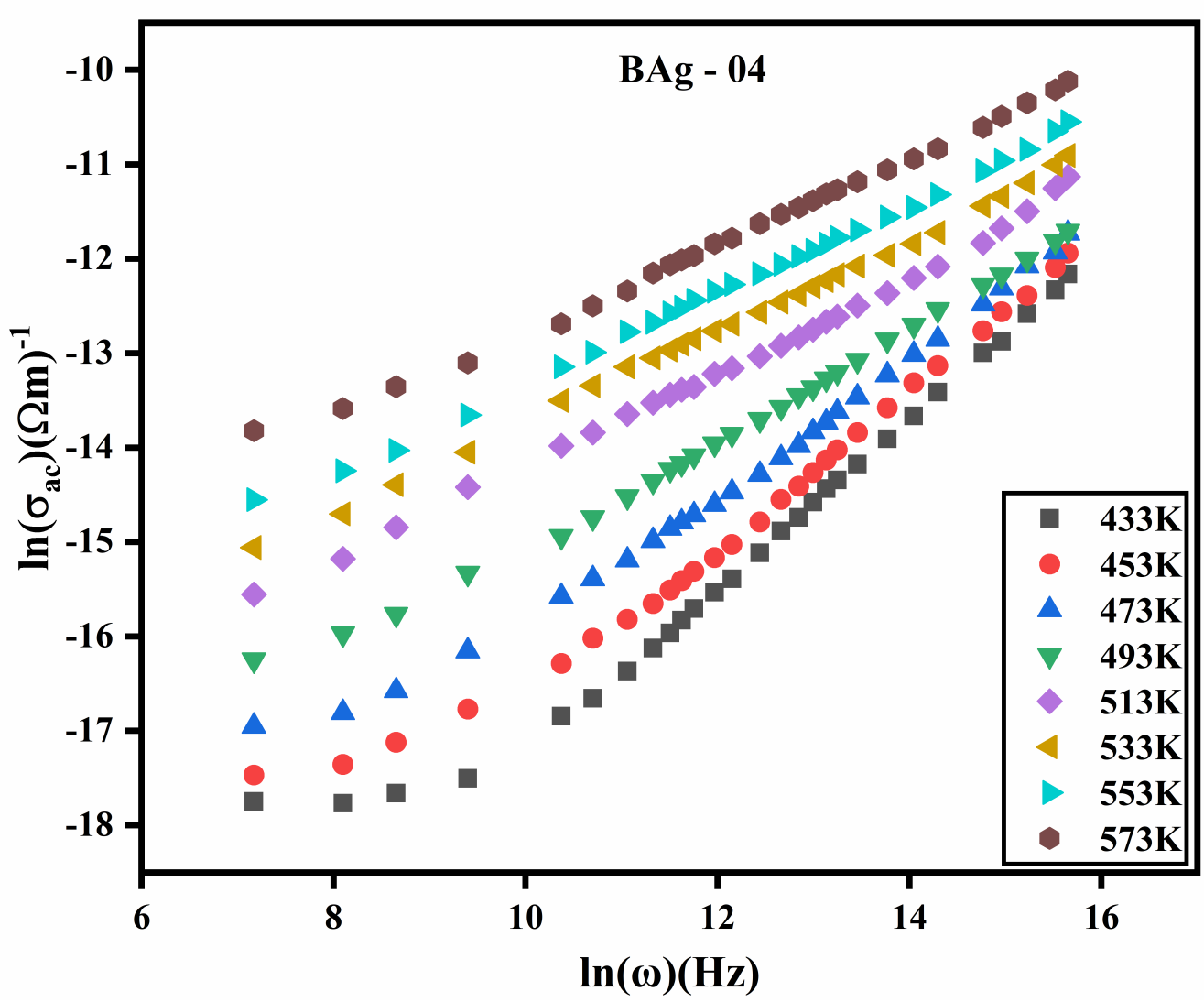

Fig 6. Plots of conductivity ln(σ_T) versus ln(ω) of the BAg-4 glass at different temperatures

contrast, the σ_{ac} remains nearly unchanged at low frequencies but exhibits a strong dependence on frequency at high-frequency region. The σ_T behavior follows Jonscher's power law relation given by

$$\sigma_T = \sigma_{\text{dc}} + A\omega^5, \text{ here } \sigma_{\text{ac}} = A\omega^5 \quad (21)$$

Where, A is the pre-exponential factor, ω denotes the angular frequency of the applied field, and s indicates the frequency exponent. A non-linear best fit to the power law relation (**Eqn. 21**) was applied to the σ_T of the prepared glass, allowing for the extraction of dc conductivity and the parameter s, of the material; s- lying between 0 to 1. By deducting the dc conductivity values from σ_T, the true ac conductivity of the prepared glass was obtained. This regression analysis was similarly conducted for all other glasses. The ac conductivity values obtained at 10 kHz and temperature 573 K are presented in Table 3. AC conductivity shows an increase from 2.328×10^{-6} to $3.457\times10^{-6}\Omega^{-1}m^{-1}$ of the present glasses, but slightly decreases at 1.2 mol% of AgCl. The enhancement in conductivity with rising AgCl concentration can be attributed to a greater number of bridging oxygen (BO) atoms and an increase in mobile charge carriers in the glass matrix[5]. The inclusion of AgCl was anticipated to enhance the ac conductivity (σ_{ac}) by contributing additional electronic pathways to the overall conductivity and altering the glass structure. The reduction in σ_{ac} at 1.2 mol% AgCl concentration can be explained by the mixed ionic-electronic (MIE) effect, which likely arises from the blocking influence of AgCl. This interference reduces the mobility of ionic charge carriers, leading to a decrease

in σ_{ac} [26]. The temperature influence on σ_{ac} was investigated utilizing Mott's small polaron hopping framework, Figure 7(a) shows that the plots of (σT) versus 1000/T of the prepared BAg glass samples. These plots exhibit a linear behavior; the slopes were then used to determine the activation energy W_{ac}. The AC activation energy (W_{ac}) at 10 kHz and 573 K for all glass specimens was determined and the values are presented in Table 3. The W_{ac} decreases from 0.484 to 0.382 eV for prepared glasses but slightly increases at 1.2 mol% of AgCl. This trend in W_{ac} shows an inverse relationship with the σ_{ac}, which aligns with similar observations reported in the literature. The decrease in W_{ac} implies a change in the prevailing conduction process from ionic to electronic, attributed to short-range electron hopping across energy barriers. This process requires less energy for charge transport, leading to lower W_{ac} values and enhanced electrical conductivity. In contrast, at 1.2 mol% AgCl, the observed reversal in behavior, marked by a rise in W_{ac} and a decline in conductivity, indicates a transition back to ionic conduction.

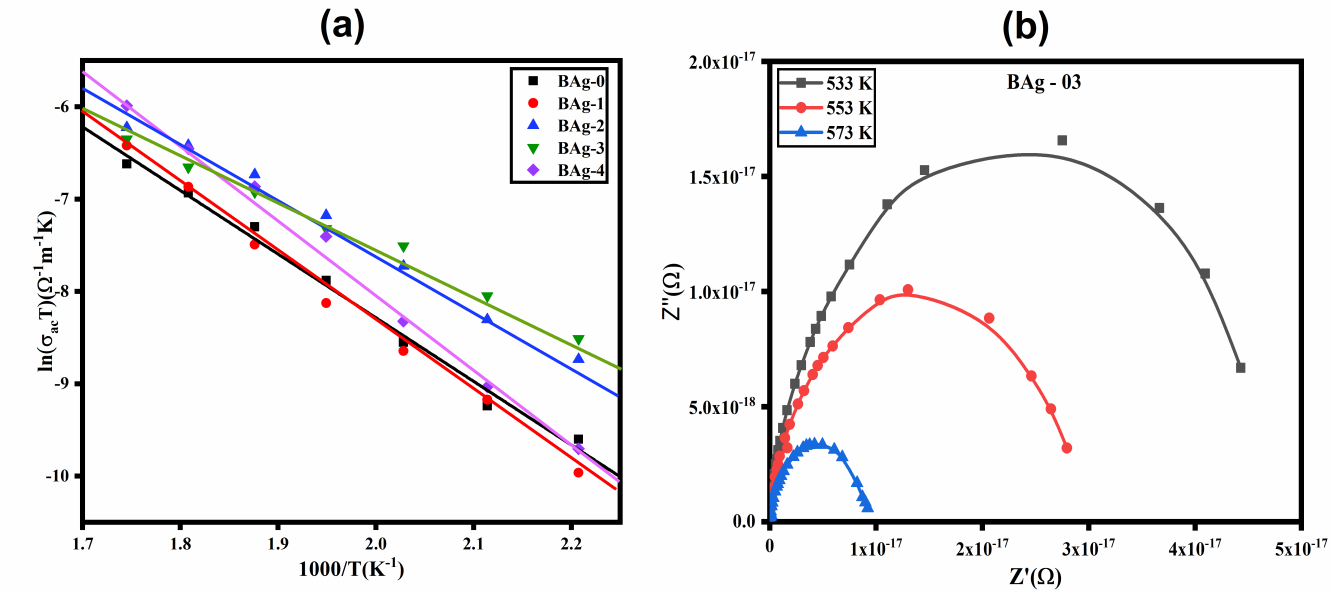

Fig 7. (a). Plots of ln(σ_{ac}T) versus 1000/T at 573 K for a frequency of 10 kHz and (b). Nyquist plots of Z'' versus Z' as a function of temperature for BAg-3 glass

3.6 Frequency exponent(s)

Since the σ_{ac} exhibits greater dispersion at higher frequencies than at lower ones, the frequency exponent was determined for all prepared glass samples. The temperature dependence of the parameter s is presented in Table 3. The s value varies broadly between 0.992 to 0.472 across all the samples and temperatures. For a given sample, s value, in general, decreases with increasing temperature. The observed change in frequency exponent with temperature is in clear disagreement with the predictions of the quantum mechanical tunneling (QMT) model, which suggests that s should be temperature independent. In contrast, the results are qualitatively consistent with the correlated barrier hopping (CBH) model, which predicts a decline in s with rising temperature.

3.7 Impendence (Z) variation

The complex impedance analysis technique accurately represents the true electrical behavior of the systems. Figure 7(b) presents the Nyquist plots of the imaginary part of the impedance (Z'') versus the real part (Z') of the BAg-3 glass composition at different fixed temperatures, illustrating their temperature dependence. These plots, known as Cole-Cole plots, appear as semicircles of varying radii, indicating that the glass behaves as a single-phase system under the entire temperature range [27]. A clear reduction in the diameter of the semicircles with increasing temperature can be observed in Figure 7(b), indicating improved conductivity of the samples. Moreover, the point where the semicircle crosses the Z' axis moves to smaller values as the temperature increases, indicating that the sample's internal resistance reduces with rising temperature. This also suggests a growth in ionic conduction losses at elevated temperatures [27], [28].

Table 3. AC conductivity (σ_{ac}), Activation energy (W_{ac}), frequency exponent (s) obtained by A non-linear fit to the power law was applied to the σ_T of the prepared glasses

Sample Codes	Frequency (f) = 10 kHz		Frequency Exponent (s) of the present glasses at different temperatures							
	(σ_{ac})(x 10^{-6} $\Omega^{-1}m^{-1}$)± 002at 573 K	Activation Energy(W_{ac}) in eV± 001 at 573 K	433 K	453 K	473 K	493 K	513 K	533 K	553 K	573 K
BAg-0	2.328	0.484	0.956	0.874	0.992	0.739	0.675	0.612	0.635	0.599
BAg-1	2.841	0.465	0.991	0.843	0.849	0.677	0.617	0.607	0.542	0.501
BAg-2	3.457	0.382	0.849	0.824	0.779	0.718	0.655	0.622	0.604	0.600
BAg-3	3.044	0.449	0.628	0.803	0.693	0.504	0.495	0.517	0.475	0.593
BAg-4	4.375	0.429	0.921	0.869	0.780	0.612	0.598	0.513	0.498	0.472

4 Conclusion

The AgCl-doped amorphous alkali borate glass samples were synthesized using the melt-quenching method to analyze the impact of AgCl nanoparticles on the physical, optical, dielectric properties, and AC conductivity. As the concentration of AgCl rose, the molar volume of the glasses dropped, while their density increased from 2.426 to 2.493 g/cm^3. The variation in optical band gaps with AgCl doping indicates that up to 1.2 mol%, the incorporation of AgCl nanoparticles increases electron localization due to a higher concentration of donor centers, leading to a reduction in both direct and indirect band gaps. However, at 1.6 mol% doping, a slight increase in the band gaps is observed, attributed to reduced electron localization and a lower concentration of donor centers, likely resulting from a decrease in non-bridging oxygens (NBOs) and subsequent structural modification within the glass network. The dielectric properties of the glasses decreased while ac conductivity showed an increase with temperature/frequency as well as with AgCl doping. The frequency dependence of ac conductivity obeyed the familiar Jonscher's power law. AgCl nanoparticles-doped lithium-borate glasses exhibit notable improvements in electrical conductivity and optical behavior when their optical characteristics and conductivity are examined. Because of these improvements, the present doped glasses show promise as potential future optoelectronic device applications.

References

1) Mirtaleb A, Wang R. Enhancing ionic conductivity in Li7P3S11 solid electrolytes via doping strategies: Implications for solid-state lithium-sulfur batteries. *Solid State Ionics*. 2025;423:116844. https://doi.org/10.1016/j.ssi.2025.116844.
2) Yao D, Wang L, Hao J, Mu J, Liang L, Hou L, et al. Entropy-Assisted Doping Strategy Enabling Chemo-Mechanically Reliable Ultrahigh-Ni Co-Free Polycrystalline Cathode for Commercializable Lithium-Ion Batteries. *ChemSusChem*. 2025;18(11):e202500067. https://doi.org/10.1002/cssc.202500067.
3) Choi H, Lee H, Lu J, Kwon SB, Jeong D, Park B, et al. Trifunctional robust electrocatalysts based on 3D Fe/N-doped carbon nanocubes encapsulating Co4N nanoparticles for efficient battery-powered water electrolyzers. *Carbon Energy*. 2024;6(6):e505. https://doi.org/10.1002/cey2.505.
4) Gui X, Xiang C, Wang S, Zhang T, Ge Z, Sun G, et al. Effect of microalloying on microstructure and mechanical properties of FeCrNi medium-entropy alloy prepared by laser metal deposition. *Journal of Alloys and Compounds*. 2025;1024:180262. https://doi.org/10.1016/j.jallcom.2025.180262.
5) Srinivas G, Srinivas B, Komaraiah D, Shareefuddin M, Sayanna R, Samudrala R. Structural, Optical and Electrical Properties of Copper Doped Alkali Borate Glasses. *Journal of Research Squire*. 2022. https://doi.org/10.21203/rs.3.rs-988680/v1.
6) Huang C, Yu J, Zhang CY, Cui Z, He R, Yang L, et al. Anionic Doping in Layered Transition Metal Chalcogenides for Robust Lithium-Sulfur Batteries. *Angewandte Chemie International Edition*. 2025;64(8):e202420488. https://doi.org/10.1002/anie.202420488.
7) Zaini N, Mohamed S, Mohamed Z. Effects of vanadium on the structural and optical properties of borate glasses containing Er3+ and silver nanoparticles. *Materials*. 2021;14(13):3710. https://doi.org/10.3390/ma14133710.
8) Keshavamurthy K, Jagannath G, Aloraini D, Almuqrin A, Sayyed M, Sathish K, et al. Silver nanoparticles amplified visible and infrared photoluminescence features of Er3+ ions activated in borate glasses. *Plasmonics*. 2023;18(1):175–182. https://doi.org/10.1007/s11468-022-01736-2.
9) Jagannathan A, Gangareddy J, Rajaramakrishna R, Rajashekara K, Rao S, Kaewkhao J, et al. Precursor based tuning of the nonlinear optical properties of Au-Ag bimetallic nanoparticles doped in oxy-fluoroborate glasses. *Journal of Non-Crystalline Solids*. 2021;561:120766. https://doi.org/10.1016/j.jnoncrysol.2021.120766.
10) Wang L, Moshwan R, Yuan N, Chen Z, Shi X. Advances and Challenges in SnTe-Based Thermoelectrics. *Advanced Materials*. 2025;37(10):2418280. https://doi.org/10.1002/adma.202418280.
11) Liu X, Zhang N, Wang P, An X, Shu J, Zhu Y, et al. Ionic conductivity regulating strategies of sulfide solid-state electrolytes. *Energy Storage Materials*. 2024;72:103742. https://doi.org/10.1016/j.ensm.2024.103742.
12) Mastanappa A, Biradar S, Devidas G, Rajaramakrishna R, Sayyed M, Chandrashekara M. Effect of Li2O on physical, structural, thermal, optical, and electrical properties of mixed alkali borate glasses containing silver nanoparticles. *Optical Materials*. 2024;157:116224. https://doi.org/10.1016/j.optmat.2024.116224.
13) Biradar S, Chandrashekara M, Dinkar A, Devidas G, Bennal A, Sayyed M, et al. A multifaceted study of B2O3-BaO-PbO-WO3 glasses doped with Bi2O3: insights from physical, thermal, structural, mechanical and optical analyses towards improved shielding properties. *Ceramics International*. 2024;50(17):29332–29345. https://doi.org/10.1016/j.ceramint.2024.05.227.

14) Gui W, Yao L, Zhou X, Wang C. Defect modulation of stable and fast inorganic perovskite Rb2AgCl3 scintillators via Li+ doping for X-ray imaging. *Journal of Alloys and Compounds*. 2025;1014:178667. https://doi.org/10.1016/j.jallcom.2025.178667.
15) Byalollikar D, Biradar S, Dinkar A, Sankarappa T, Biradar J. Impact of bismuth oxide on structural, optical and gamma-ray shielding properties of calcium–sodium–borate glasses. *Radiation Protection Dosimetry*. 2024;200(11-12):1207–1215. https://doi.org/10.1093/rpd/ncae066.
16) Dimitrov V, Sakka S. Linear and nonlinear optical properties of simple oxides. II. *Journal of Applied Physics*. 1996;79(3):1741–1745. https://doi.org/10.1063/1.360963.
17) Malge A, Sankarappa T, Sujatha T, Devidas G. Structural, Dielectric and AC Conductivity of Multicomponent Borotellurite Glasses. *Glass Physics and Chemistry*. 2021;47(S1):S1–S9. https://doi.org/10.1134/S1087659621070038.
18) Biradar S, Dinkar A, Devidas G. Optical Modifications in Eu2O3-Doped Borate Glasses: Impact on Bandgap, Metallicity, and Photonic Properties. *Nexus of Future Materials*. 2024;p. 588347. https://doi.org/10.70128/588347.
19) Ahmad A, Hashim S, Ghoshal S. Physical, thermal and absorption traits of lithium strontium zinc borate glasses: Sensitiveness on Dy3+ doping. *Journal of Alloys and Compounds*. 2020;844:156176.
20) Mansour A, Hammad AA, Nahrawy AE. Sol–gel synthesis and physical characterization of novel MgCrO4-MgCu2O3 layered films and MgCrO4-MgCu2O3/p-Si based photodiode. *Nano-Structures & Nano-Objects*. 2021;25:100646. https://doi.org/10.1016/j.nanoso.2020.100646.
21) Nahrawy AE, Bakr A, Hammad AA, Mansour A. Nano-architecture of CaO/Ag-chitosan nanocomposite by sol gel process: formation and characterization. *Egyptian Journal of Chemistry*. 2021;64(12):7393–7406. https://doi.org/10.21608/ejchem.2021.80608.3995.
22) Nahrawy AE, Hammad AA, Mansour A. Compositional effects and optical properties of P2O5 doped magnesium silicate mesoporous thin films. *Arabian Journal for Science and Engineering*. 2021;46(6):5893–5906. https://doi.org/10.1007/s13369-020-05067-4.
23) Nahrawy AE, Hammad AA, Mansour A. Preparation and characterization of transparent semiconducting silica nanocomposites doped with P2O5 and Al2O3. *Silicon*. 2021;13(10):3733–3739. https://doi.org/10.1007/s12633-021-00962-3.
24) Prabhudessai A, Balaji S, Prasad S, Chahal S, Biswas K, Ramesh K, et al. Thermal, structural, and conductivity properties of As14Sb26S (60— x)–(AgI) x chalcogenide glasses. *Journal of Applied Physics*. 2024;135(9). https://doi.org/10.1063/5.0174873.
25) El-Menyawy E, Zedan I, Mansour A, Nawar H. Thermal stability, AC electrical conductivity and dielectric properties of N-(5-{[antipyrinyl-hydrazono]-cyanomethyl}-[1, 3, 4] thiadiazol-2-yl)-benzamide. *Journal of Alloys and Compounds*. 2014;611:50–56. http://dx.doi.org/10.1016/j.jallcom.2014.05.120.
26) Mohamed S, Halimah M, Subban R, Yahya A. AC conductivity and dielectric properties in mixed ionic–electronic 20Na2O–20CaO–(60–x) B2O3–xV2O5 glasses. *Physica B: Condensed Matter*. 2021;602:412480. https://doi.org/10.1016/j.physb.2020.412480.
27) Mohansingh H, Sankarappa T, Malge A, Devidas A, Raghavendra B. Dielectric relaxation studies in WO3 mixed lead vanadate glasses. *Materials Today: Proceedings*. 2023;80:933–936. https://doi.org/10.1016/j.matpr.2022.11.330.
28) Choi Y, Lee Y, Ahn H, Jeong J, Chung K, Scanlon D, et al. Exploring dopant-enhanced ionic conductivity of AgCl-doped Li7P3S11 solid electrolytes: Integrating synchrotron Rietveld analysis, DFT, and ANN-based molecular dynamics approaches. *Carbon Energy*. 2024;6(11):e564. https://doi.org/10.1002/cey2.564.